Journal of Natural Gas Science and Engineering 33 (2016) 599–610

Contents lists available at ScienceDirect

Journal of Natural Gas Science and Engineering

journal homepage: www.elsevier.com/locate/jngse

Controls on matrix permeability of shale samples from Longmaxi and Niutitang formations, China

Hongyan Qu [a, b, c, *], Zhejun Pan [d], Yan Peng [e], Fujian Zhou [c]

[a] State Key Laboratory of Petroleum Resources and Prospecting, China University of Petroleum, 18 Fuxue Road, Changping, Beijing, 102249, China
[b] State Key Laboratory of Geomechanics and Geotechnical Engineering, Institute of Rock and Soil Mechanics, Chinese Academy of Sciences, Wuhan, 430071, China
[c] Unconventional Natural Gas Institute, China University of Petroleum, 18 Fuxue Road, Changping, Beijing, 102249, China
[d] CSIRO Energy, Private Bag 10, Clayton South, Victoria 3169, Australia
[e] School of Mechanical and Chemical Engineering, University of Western Australia, WA, Australia

ARTICLE INFO

Article history:
Received 10 January 2016
Received in revised form
17 May 2016
Accepted 18 May 2016
Available online 20 May 2016

Keywords:
Matrix permeability
Longmaxi and Niutitang shale
Pressure-decay permeability measurement
Geological and geochemical control
Pore-size distribution
Permeability-porosity model

ABSTRACT

The Lower Silurian Longmaxi shale and the Lower Cambrian Niutitang shale are typical marine shales in China, promising for shale gas production, whereas the gas production from these two formations vary considerably because of the different flow properties determined by geology and lithology conditions. Matrix permeability, compared with fracture permeability, is an important factor controlling the long-term gas production from shale gas reservoirs. However, matrix permeability is difficult to measure at field due to the constrained measuring conditions. In this study, the Pressure-decay method was applied to measure the matrix permeability of the relatively high permeability Longmaxi and low permeability Niutitang shales. Moreover, controls of geochemical and geological factors on the matrix permeability were investigated for these two gas shales, differing in buried depth, porosity, Total Organic Carbon (TOC) contents and thermal maturity. Furthermore, the effects of dominant controlling factors on the matrix fluid conductivity were analyzed. Results show that matrix permeability increases with TOC content at different rates for Longmaxi and Niutitang shales. The difference in pore structure and pore-size distribution between the two shales is the main reason for the different matrix permeability and gas production. In addition, the development of organic nano pores with the partial fill-in of the minerals in the Niutitang shale was observed through the Scanning Electron Microscope (SEM), accounting for the contradiction of high porosity and low matrix permeability in the Niutitang shale. The precise determination of intermediate parameter in the Pressure-decay method is the key control for the accuracy of matrix permeability measurement and our study improves the understanding of the importance of pore-size distribution on flow properties in the matrix of shale gas reservoirs.

1. Introduction

Great breakthrough has been achieved in shale gas exploration and production in Sichuan Basin, China, where the Lower Silurian shale and the Lower Cambrian shale are two of the most promising thermally mature marine shales with great potential due to the rich organic matter, moderate porosity and high brittleness (Ma et al., 2015; Wang et al., 2013b; Wei et al., 2012). High output has been achieved in the Lower Silurian Longmaxi Formation with accumulative production over 1.2 billion m^3 in the Fuling gas field till 2015, whereas shale gas production rates are low in many of the exploratory drilling efforts targeting the Lower Cambrian Niutitang shale and high gas production only occurred in few parts of the Niutitang Formation (Wang et al., 2015).

Well productivity is affected by many factors including shale matrix properties (Pan and Connell, 2015), which especially influences the long-term producibility of the reservoir and is dependent on the pore network of the matrix. The different gas production behavior between the Longmaxi and Niutitang shales may result from their difference in the geological and geochemical properties as well as petrophysical characteristics. Both Longmaxi

* Corresponding author. Unconventional Natural Gas Institute, China University of Petroleum, 18 Fuxue Road, Changping, Beijing, 102249, China.
E-mail addresses: hongyan.qu@cup.edu.cn (H. Qu), zhejun.pan@csiro.au (Z. Pan), 21364783@student.uwa.edu.au (Y. Peng), zhoufujian@263.net (F. Zhou).

http://dx.doi.org/10.1016/j.jngse.2016.05.054
1875-5100/

and Niutitang formations are organic-rich black shales. For Longmaxi Formation, Total Organic Carbon (TOC) content ranges from 0.14% to 18.4%, clay mineral content varies between 14.3% and 70% and vitrinite reflectance (R_o) ranges from 1.8% to 4.2% (Chen et al., 2014; Dai et al., 2014; Pan et al., 2015a; Pu et al., 2015). Compared with the Longmaxi shale, the Niutitang shale has higher TOC content and depositional thickness as well as wider distribution areas (Liang et al., 2008), suggesting high potential of gas production. Specifically, its TOC content ranges from 0.1% to 14.3%, clay mineral content varies between 6.2% and 62.4% and vitrinite reflectance ranges from 0.69% to 4.53% (Yang et al., 2014; 2015a; 2015b; Yang and Xu, 2015).

Apart from the structural complexity and low gas content, the different petrophysical properties may considerably account for the low gas production in Niutitang and relatively high gas production in the Longmaxi Formation because porosity and permeability are the critical parameters determining gas-bearing and gas-developing in shale (Zou et al., 2011; Wang et al., 2013c; Zhang et al., 2008a; 2008b; 2010). Researches show that porosity and permeability are of great difference for the Longmaxi and Niutitang shales. For Longmaxi shale, literature data show that porosity could range between 1.2% and 10.8% and permeability could vary from 15.0 nD to 1.74 mD (Dai et al., 2014; Pan et al., 2015a), while for Niutitang shale, porosity and permeability can be as high as 16.51% and 0.11 mD, and as low as 0.1% and 0.001 nD, respectively (Yang et al., 2014; 2015a; 2015b; Yang and Xu, 2015).

Shale permeability is generally controlled by geological properties including shale fabric, porosity, lithology, and microfractures/microcracks (Aplin et al., 1995; Dewhurst et al., 1999a; 1999b; Kwon et al., 2004; Lash and Engelder, 2005; Schlomer and Krooss, 1997; Yang and Aplin, 2007; Ghanizadeh et al., 2013), as well as geochemical properties such as the organic matter content, thermal maturity and fracture spacing (Soeder, 1988). It is also affected by the stress conditions. Specifically, shale permeability increases with porosity (Loucks et al., 2009), which increases with TOC and quartz content while decreases with clay content (Wu et al., 2014). In addition, matrix permeability is related to thermal maturity. Compared with immature and overmature shales, the lowest permeability was normally found in intermediately matured shales (445 °C < T_{max}<449 °C; vitrinite reflectance in the range of 0.88%–1.01%) (Ghanizadeh et al., 2013). Therefore, the relatively high thermal maturity of the Niutitang shale may result in the poor development of organic matter hosted pores and lead to low permeability (Tian et al., 2015; Wang et al., 2013a). Moreover, matrix permeability is affected by pore-size distribution. Experiments on the Devonian gas shale in North America show that samples with high permeability not only contain high quartz and TOC, moderate clay but also are characterized with balanced ratios among micro-, meso- and macroporosity due to greater propensity to fracture and communication between macropores and micropores in the organic and clay fractions (Chalmers et al., 2012). Nevertheless, gas shales in the North America distinguish from those marine shales in China in the geological properties, pore network and fracture distribution, which may result in different petrophysical characteristics and flow behavior. The effects of geological and geochemical properties on shale matrix permeability of Longmaxi and Niutitang shales in China still have not been well studied.

Therefore, in this study, controls on matrix permeability were investigated for the Lower Silurian Longmaxi and the Lower Cambrian Niutitang gas shales from the Sichuan Basins, China. Matrix porosity and permeability were mainly measured with Pressure-decay method, combined with the Pulse-decay method. Moreover, dominant geochemical and geological factors including TOC content, porosity, and permeability sensitivity to confining pressure of shale samples from these two formations were examined through a series of parameter-characterization. Furthermore, pore-size distribution and pore structure were analyzed through the high-pressure mercury injection and Scanning Electron Microscope (SEM) observations, and their effects on matrix permeability were studied. Our study aims to improve the understanding of reasons behind different outputs from Longmaxi and Niutitang shales in Sichuan Basin and provide guidance for the shale gas developments in Southwest China.

2. Experiments and methodology

2.1. Sample preparation

A total of 12 samples were obtained from the Lower Silurian Longmaxi (six samples) and the Lower Cambrian Niutitang (six samples) formations in Sichuan Basin, located in Southwest China. Black shales are widely distributed in these two formations, deposited in a marine environment and widespread in the Yangtze Platform, South China (Zhang et al., 2008a; 2008b; 2010; Wang, 2014). They are two of the main target formations for shale gas exploration in China. The Cambrian Niutitang Formation has fairly consistent thickness across the Sichuan Basin, averaging about 120 m thick and 2800 m deep (Feng et al., 2013), while bioclastic cherty black shale mixed with gray silty mudstones developed in the shelf sedimentary environment for the Longmaxi Formation (EIA, 2013), with black shale ranging between 10 and 170 m (Chen et al., 2014).

Core samples of Niutitang Formation were obtained from outcrops while samples of the Longmaxi shale were collected from three production wells in the depth between 700 m and 900 m where commercial shale gas production has been achieved. Among the 12 samples, six samples (three from each formation) were drilled perpendicular or parallel to bedding and sub-cored to plugs of 2.5 cm–5 cm long and 2.54 cm in diameter. The cleaned/dried core plugs were used for helium porosimetry and permeability test. The other six samples were crushed to small particles and sieved to 20/40 mesh for the matrix permeability measurements. Matrix permeability was measured 'as-received' without any further treatment.

2.2. Geochemical property and pore structure analyses

Sampling represents a variation in TOC, pore structure and porosity so that their controls on matrix permeability can be examined. Sample offcuts were prepared as small blocks and slices and a series of experiments were conducted to characterize the geochemical properties and the pore system of the Niutitang and Longmaxi black shales. The TOC contents were analyzed through a Leco carbon-sulfur analyzer. The vitrinite reflectance was measured using a Leitz MVP-3 microscope photometer. Pore structure was observed through SEM and quantitatively characterized by Mercury Injection Capillary Pressure (MICP) and nitrogen adsorption from macropore to micropore, and the pore-size distribution (PSD) were analyzed. All analyses were performed at China University of Petroleum (Beijing) and the Chongqing Mineral Resources Supervision and Test Center.

2.3. Gas permeability measurements

Shale permeability can be measured through several methods, based on different physical principles and utilizing core samples at different scales (Ghanizadeh et al., 2013; 2014a; 2014b). The variation in sample size, preparation process and experimental conditions results in a wide range of permeability estimates. Traditional

steady flow techniques is impractical for shale matrix permeability measurement because very precise equipment is required due to the tight nature of shale where gas flow is slow (Carles et al., 2007; Jones, 1994; 1997). Consequently, the Pulse-decay method on core plugs and the Pressure-decay method on crushed samples, based on the non-steady-state theory, are two widely used methods for matrix permeability measurements in low-permeability shale (Chalmers et al., 2012; Cui et al., 2009; Luffel et al., 1993; Metwally and Sondergeld, 2011). Since the two techniques differ in measurement conditions and size of rock samples, there is usually a discrepancy in the measurement results between them. The Pulse-decay permeability values are consistently higher or equal to the Pressure-decay permeability values, depending on lithology and the effective stress applied in the Pulse-decay permeability measurements (Cui et al., 2013; Cui and Brezovski, 2013; Ghanizadeh et al., 2015; Suarez-Rivera et al., 2012). However, although the inconsistency in shale permeability has been acknowledged (Tinni et al., 2012), the reasons behind have not been well investigated. The unreliable shale matrix permeability measured at laboratory may lead to enormous difficulty on the reservoir evaluation and stimulation design for hydraulic fracturing, impeding the enhancement of shale gas production. Therefore, in this work, permeability measured using both the Pressure-decay method and Pulse-decay method were studied and compared for the samples differing in TOC content and pore network characteristics from Longmaxi and Niutitang shales.

2.3.1. Pressure-decay permeability measurements on crushed samples

The individual crushed shale particles are assumed to contain few or no micro-fractures compared with plugs because samples are likely to break along micro fractures and bedding planes during crushing (Luffel et al., 1993). Therefore, the Pressure-decay method is capable of providing a better estimation of matrix permeability compared to other methods (Ghanizadeh et al., 2015). The Pressure-decay method on crushed shale samples was applied to measure the Longmaxi and Niutitang shale matrix permeability.

Pressure-decay permeability measurements were performed on crushed shale samples with an in-house developed matrix permeameter at China University of Petroleum (Beijing) using a mean gas pressure of 1.55 MPa. Gas was injected into the unconfined crushed particles (20/40 US mesh size; 0.55 mm–0.84 mm), as shown in Fig. 1, and the decay of a subsequent pressure-pulse was recorded to calculate the matrix permeability based on the 'late-time' model (Cui et al., 2009).

Matrix permeability can be determined by the following equation (Cui et al., 2009),

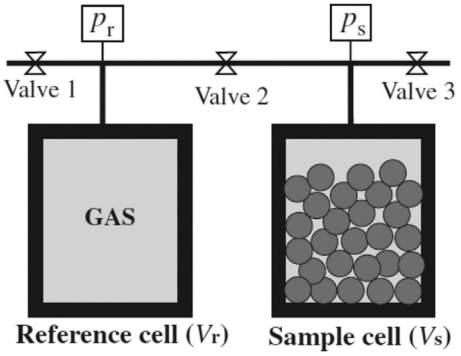

Fig. 1. Schematic procedure of Pressure-decay method (Cui et al., 2009).

$$km = \frac{R_a^2(\varphi + (1-\varphi)K_a)\mu C_g S_1}{\alpha_n^2} \tag{1}$$

where R_a is the diameter of the crushed particle; φ is the porosity; k_m is the matrix permeability; μ is the gas viscosity; α_n is the nth root of an intermediate equation; K_a is the density ratio of adsorbed gas to free gas, which differs according to the type of experimental gas, and needs to be corrected; c_g is the gas compressibility; and S_1 is the intermediate parameter, determined by the slope of the pressure decay.

In the matrix permeability measurement, bulk density is a key input parameter to calculate the S_1, which considerably affects the accuracy of the results. The bulk density can be determined by the bulk volume. Nevertheless, since the size of crushed sample is too small, the implementation of immersion technique for bulk volume measurement on crushed samples is experimentally difficult and not applicable. In this study, the bulk density was determined through the mercury intrusion and the initial intrusion pressure was carefully selected to avoid the accumulated error in the matrix permeability determination.

2.3.2. Pulse-decay permeability measurements on core plugs

Pulse-decay permeability measurements were performed on shale plugs from Longmaxi and Niutitang shales at controlled effective stress conditions using a permeability rig developed at CSIRO (Pan et al., 2010; 2015b). The transient method developed by Brace et al. (1968) was applied in the measurements. A differential pressure of 1 MPa was initially applied between upstream and downstream of the shale sample at a series of controlled confining pressures of 3 MPa, 5 MPa, 7 MPa and 9 MPa. Permeability was calculated according to the decay of the differential pressure across the shale sample (Brace et al., 1968; Pan et al., 2010; 2015b). The differential pressure decay curve can be modeled as follows,

$$\frac{(P_u - P_d)}{(P_{u,0} - P_{d,0})} = e^{-\alpha t} \tag{2}$$

where $P_u - P_d$ is the pressure difference between the up- and down-stream cylinders; $P_{u,0} - P_{d,0}$ is the pressure difference between the up- and down-stream cylinders at initial stage, t is time and α is described below:

$$\alpha = \frac{k}{\mu\beta L^2} V_R \left(\frac{1}{V_u} + \frac{1}{V_d}\right) \tag{3}$$

where k is permeability; β is the gas compressibility; L is the sample length; V_R is the sample volume; V_u and V_d is the volume of the up- and down-stream cylinder, respectively (Pan et al., 2010).

The experimental uncertainty of permeability measurement is approximately 5%, similar to that in Ghanizadeh et al. (2014a; 2014b) as the experimental setup and procedure are similar.

3. Results and discussion

3.1. Characterization of geological and geochemical properties

Results pertaining to the buried depth, organic richness, porosity and median pore-throat radius of the samples from Longmaxi and Niutitang shales are presented in Table 1. The TOC content of the Longmaxi shale samples ranges from 1.71 wt % to 3.35 wt % while it is in the higher range between 4.44 wt % and 5.25 wt % for the Niutitang shale samples. The median pore-throat radius was determined from the mercury intrusion curve, varying from 4.4 nm to 5.8 nm for the Longmaxi shale and ranging between

Table 1
Geochemical and geological property characteristics of shale samples from Longmaxi and Niutitang formations.

Sample number	Buried depth (m)	Weight of crushed samples (g)	TOC (wt. %)	Porosity (%)	Median pore-throat radius (nm)
L#1	769.69	27.92	1.71	1.49	5.8
L#2	861.23	28.13	2.50	2.05	5.6
L#3	900.33	28.42	3.35	3.39	4.4
N#1	Outcrop	41.65	4.44	3.25	3.9
N#2	Outcrop	42.79	4.73	4.62	3.8
N#3	Outcrop	42.75	5.25	5.18	4.5

3.8 nm and 4.5 nm for the Niutitang shale at a series of intrusion pressures from 0.01 MPa to 413.79 MPa.

The micropore structures are normally identified by the shape of mercury capillary pressure curve and speculated by the hysteresis loop of mercury intrusion and nitrogen adsorption analysis. Since mercury is non-wetting liquid, it invades into shale pores as the intrusion pressure exceeds the capillary pressure. According to the capillary theory, the capillary pressure is small for the macropores, while large for the meso- and micropores because the capillary pressure is inversely proportional to the pore radius. The amount of incremental mercury intrusion at certain pressure could be approximately referred as the volume of pores with corresponding size.

The evolutions of incremental intrusion of mercury into shale samples with intrusion pressure, as shown in Figs. 2 and 3, indicate that the pore-size distributions of Longmaxi and Niutitang shales are of great difference. The amount of mercury intruding into Longmaxi samples at low pressures (0–0.69 MPa) is larger than that into Niutitang samples, as shown in Fig. 2. Specifically, the largest incremental intrusion amounts into the Longmaxi shale samples are higher than 0.001 mL/g while those into the Niutitang shale samples are between 0.0004 mL/g and 0.0006 mL/g. This difference between Fig. 2(a) and (b) indicates that macropores developed better in the Longmaxi samples compared with those in the Niutitang samples.

The difference in the distribution of meso- and micropores between Longmaxi and Niutitang samples is shown in Fig. 3. The incremental amounts of mercury intrusion remain relatively low and increase slightly as pressure increases from 0.69 MPa to 68.97 MPa, indicating that the amounts of mesopores are small and almost the same for both Longmaxi and Niutitang samples.

At high pressures (over 68.97 MPa), noticeably, the amount of mercury intruding into the Niutitang samples is much larger than that into the Longmaxi samples. Specifically, the largest incremental intrusion amount into the Longmaxi shale samples is approximately 0.0002 mL/g while that into the Niutitang shale samples is up to 0.0008 mL/g, four times of the amount into the Longmaxi shale. The difference between Fig. 3(a) and (b) demonstrates that the development of micropores in the Niutitang samples is better than that in the Longmaxi samples.

In each shale, similar trends of pore-size distribution are shown for all the three samples. However, different magnitudes can be observed among these samples, indicating the heterogeneity of the shale samples for the pore-size distribution in both shales. In the group of Niutitang samples, the amount of micropores of sample N#1 and N#2 is larger than that of N#3, while sample N#1 develops the smallest amount of macropores. Different incremental intrusion magnitude is also found among the Longmaxi samples. L#2 develops the largest amount of macropores and the amount of micropores are almost the same for all the three samples.

Fig. 4 illustrates the cumulative mercury intrusion and extrusion capillary curves of samples from Longmaxi and Niutitang shales. The cumulative mercury curves of all samples exhibit considerable hysteresis between intrusion and extrusion. The existing hysteresis shows that not all the mercury intruding into the samples can flow out during mercury extrusion process. The difficulty for mercury flowing out of samples results from the high capillary pressure, demonstrating low ratio of throats to pores in these samples. The mercury intrusion curve of each Longmaxi sample (Fig. 4(a)) illustrates a dramatic increase at low pressures, followed by a slight increase with the increasing pressure, indicating that the majority of pores in the Longmaxi samples are macropores. In contrast, the

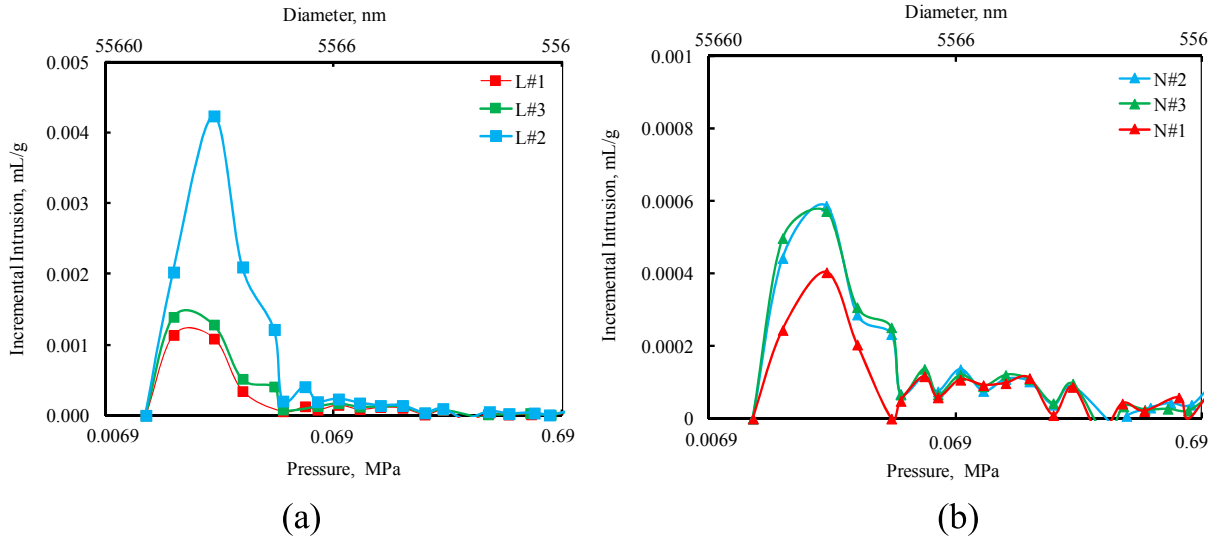

Fig. 2. Comparison of macro pore-size distribution of Longmaxi and Niutitang shale samples (a. Longmaxi samples, b. Niutitang samples).

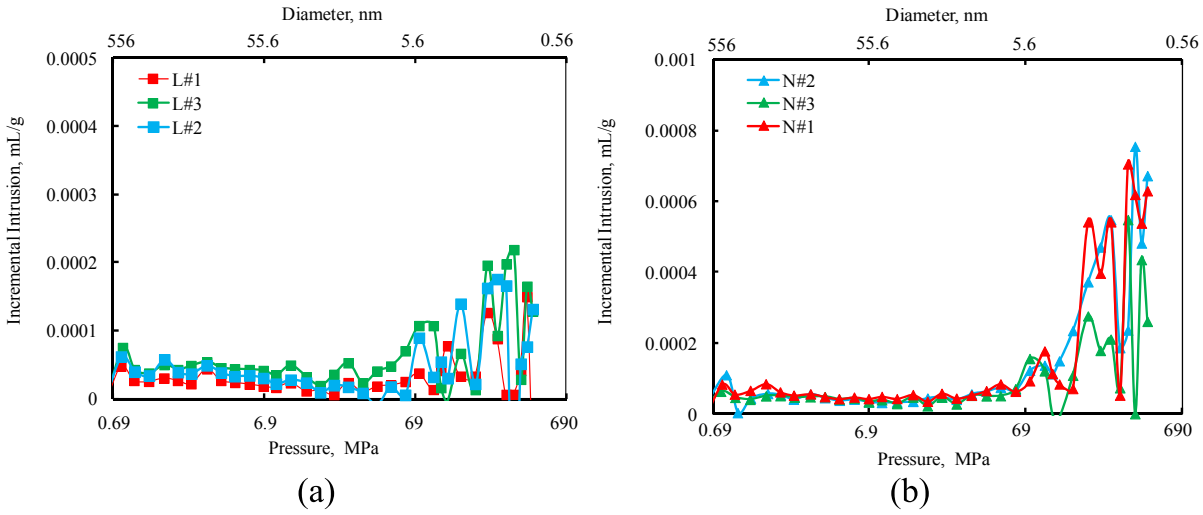

Fig. 3. Comparison of meso and micro pore-size distribution of Longmaxi and Niutitang shale samples (a. Longmaxi samples, b. Niutitang samples).

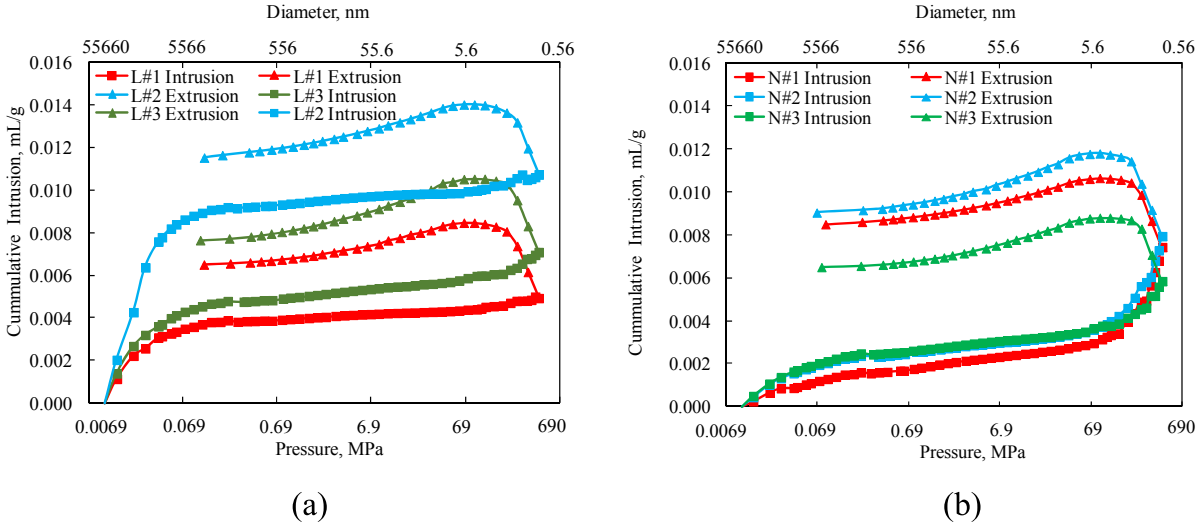

Fig. 4. Comparison of cumulative mercury intrusion and extrusion curve of Longmaxi and Niutitang samples (a. Longmaxi samples, b. Niutitang samples).

mercury intrusion curve of each Niutitang sample (Fig. 4(b)) experiences a graduate increase at low pressures and then a sharp increase at high pressures (over 68.97 MPa), demonstrating that the majority of pores in the Niutitang samples are micropores.

The main contributors to matrix permeability and porosity of Longmaxi and Niutitang samples can be speculated from the pore-size distribution. The matrix permeability and porosity of Longmaxi samples is mainly attributed to the macropores while in the Niutitang samples the meso- and micropores contribute the most to the gas flow. These characteristics obtained from the mercury intrusion and extrusion curves have been applied to modify the matrix permeability-porosity model proposed in the later section of this study.

3.2. Comparison of matrix permeability among Longmaxi, Niutitang and other shales

Variations of measured matrix permeability with porosity of crushed samples from Longmaxi and Niutitang shales in Sichuan Basin, China were compared with those of other typical marine shales such as Barnett shales and other shales in the North America,

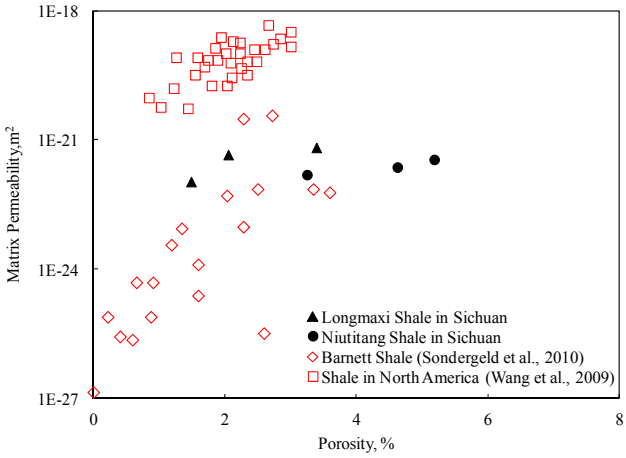

Fig. 5. Comparison of matrix permeability with porosity among crushed samples from Longmaxi shale, Niutitang shale, Barnett shale and shale in North America.

as shown in Fig. 5. Matrix permeability of Longmaxi and Niutitang shales is relatively high compared with that of Barnett Shales, but lower than that of the North America shales. The different matrix permeability ranges of these shales result from the controlling effects of geological and geochemical factors. The permeability at lower porosity indicates that shale is prone to being compacted by preferential collapse of those large pores which contribute most to the fluid flow (Borst, 1982; Yang and Aplin, 1998, 2007; Dewhurst et al., 1998, 1999a,b).

3.3. Effect of TOC on porosity and matrix permeability

To understand the effects of geochemical factors on porosity and matrix permeability, the variations of porosity and matrix permeability with TOC were investigated in this section. The porosity and matrix permeability of the Longmaxi and Niutitang samples are compared in Figs. 6 and 7, respectively. Porosity increases with the increasing TOC for both samples, whereas most of the porosity of the Niutitang samples is higher than that of the Longmaxi samples. Specifically, porosity increases from 1.49% to 3.39% as TOC increases from 1.71% to 3.35% for the Longmaxi samples while for the Niutitang samples it increases from 3.25% to 5.18% as TOC increases from 4.44% to 5.25%.

Matrix permeability increases with the increasing TOC for the two groups of shale samples as well. However, matrix permeability varies considerably for the Longmaxi samples and it changes as much as 0.56 nD as TOC increases from 1.71% to 3.35% while it increases less than 0.20 nD for the Niutitang samples as TOC increases from 4.44% to 5.25%. The high porosity and low matrix permeability in the Niutitang shale may account for the low gas production, partially confirmed by the pore-size distribution in section 3.1 and the SEM observation in section 3.4.

3.4. Pore structure characterization through SEM observation

The presence of complex organic and mineral pores in the Longmaxi and Niutitang shale samples was observed through the SEM, as shown in Fig. 8. There are generally five types of pores in shale, including organic nanopores, pores in clay minerals, intraparticle pores of matrix minerals, intragranular pores from microfossils, and microfractures (Feng et al., 2013). The organic and clay mineral pores develop together for the relatively high-matured

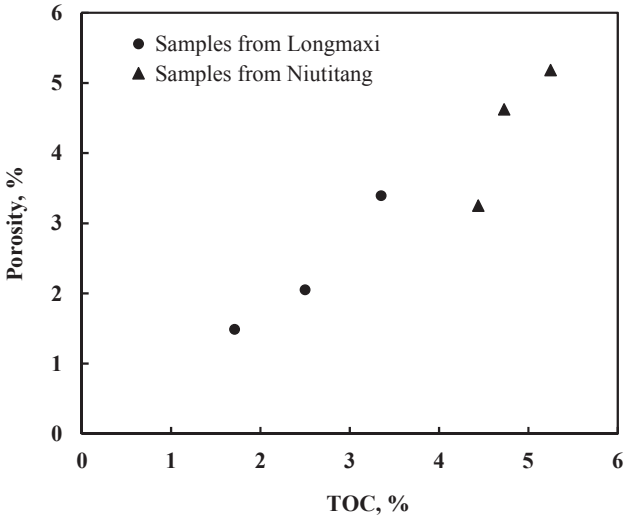

Fig. 6. Comparison of porosity variation with TOC of Longmaxi and Niutitang samples.

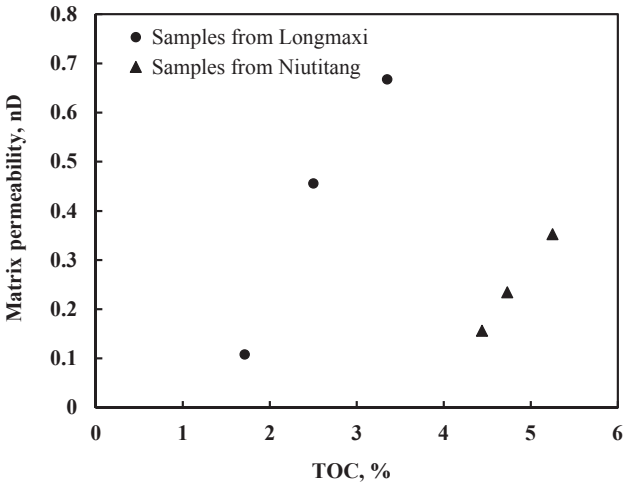

Fig. 7. Comparison of matrix permeability variation with TOC of Longmaxi and Niutitang samples.

Longmaxi and Niutitang shales and dominate the pore types.

In general, the organic matter (OM) develops in both Longmaxi and Niutitang shales. However, the organic pore development is different among the three samples in each group. As shown in Fig. 8(a), organic pores develop well in the sample L#2 and L#3, while the organic matter distributes sparsely and few organic pores are observed in the sample L#1. Compared with the Longmaxi group, the scale and quantity of the OM-hosted pores in Niutitang shale samples are relatively poor. For the sample N#1, organic matter develops with few or no pores. However, organic pores develop better in the sample N#2 and N#3 with different pore sizes. Pores with diameters under 200 nm are commonly observed in the sample N#2 while pore diameters are originally in the range of 200 nm–600 nm in the sample N#3, as shown in Fig. 8(b). Noticeably, minerals always develop with the organic matter in the Niutitang shale samples. Most of the organic pores are half or partially filled with minerals, resulting in the decrease of pore volume and pore size.

The most important features for the hydrocarbon exploration are the pore networks and their connectivity. For the Longmaxi shale samples, the organic matter develops well and the organic pores are distributed consistently, resulting in high porosity and high matrix permeability. In contrast, though pores are observed in some of the Niutitang shale samples, many of them are surrounded by or partially filled with minerals, or few pores develop due to the over-maturity of the organic matter, reducing the matrix permeability and diminishing the final gas production.

3.5. Relationship between matrix permeability and porosity

The permeability of fine-grained shale and its relationship with porosity are critical to the quantification of the long-term shale gas production (Luffel et al., 1993). Many permeability models have been proposed (Walsh and Brace, 1984; Bethke, 1989; Berryman, 1992; Nelson, 1994), relating permeability to geometric parameters, such as the hydraulic radius and porosity.

Previous studies have shown that fine-grained clastic sediment permeability is roughly related to porosity or void ratio by log-linear functions (Mesri and Olson, 1971; Lapierre et al., 1990; Nagaraj et al., 1994; Yang and Aplin, 1998; 2007; Dewhurst et al., 1998; 1999a; 1999b). However, for shale there are few simple relationships between permeability and porosity. Current permeability–porosity relationships for fine-grained shale are

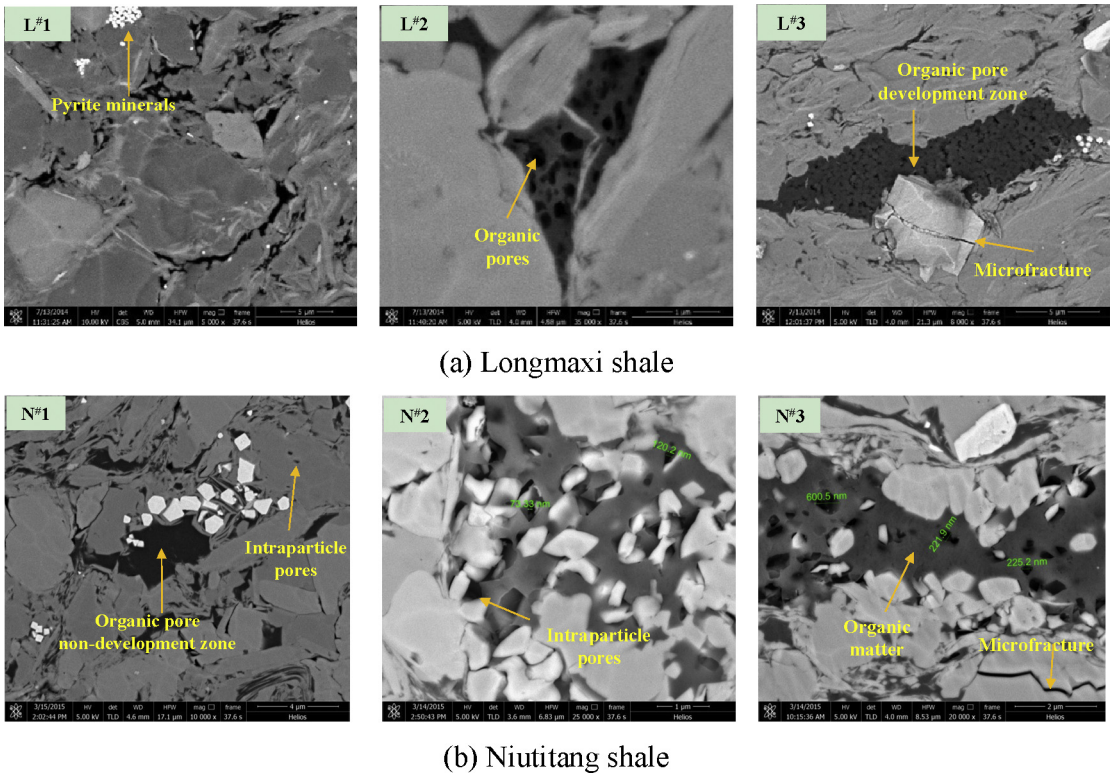

Fig. 8. SEM images of mineral and organic nanopores of samples from Longmaxi and Niutitang shales.

inadequate over the narrow range of porosity (Nagaraj et al., 1994). The wide range of permeability and the lack of a reliable permeability–porosity relationship impede quantitative reservoir characterization and flow modelling for shale gas production.

In this section, the permeability-porosity model proposed for the coal seams was first applied to calculate the shale permeability. For a porous media composed of parallel tubes with equal diameter, permeability is normally calculated by the following equation (e.g. Pan and Connell, 2012),

$$k_i = \frac{b_i^3}{12a_i} \tag{4}$$

where k_i is the permeability; b_i is the pore aperture and a_i represents the pore spacing, in the i direction.

For the anisotropic case, porosity can be written as,

$$\varphi = \frac{b_1}{a_1} + \frac{b_2}{a_2} + \frac{b_3}{a_3} \tag{5}$$

where under isotropic conditions, $\varphi = 3b/a$, therefore $a = 3b/\varphi$.

Substituting the expression of a into Eq. (4), permeability can be expressed as following,

$$k = \frac{1}{96}a^2\varphi^3 \tag{6}$$

The pore spacing was calculated through porosity and the median pore-throat radius obtained from the experiments, as shown in Table 1, and the variations of pore spacing changing with porosity are illustrated in Fig. 9. Average pore spacing of Longmaxi shale samples is approximately half order of magnitude higher than that of the Niutitang shale samples. Permeability was calculated through Eq. (6) according to the pore spacing and porosity, and the calculated permeability values are compared with the measured ones to match the experimental data, as shown in Fig. 10.

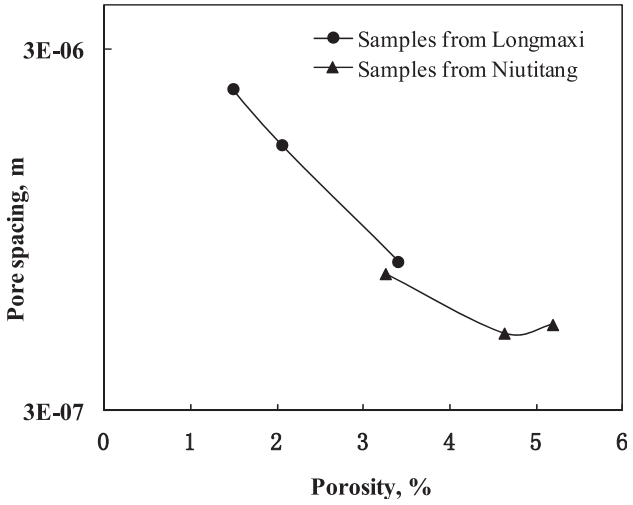

Fig. 9. Pore spacing variations with porosity of samples from Longmaxi and Niutitang shales.

Fig. 10 illustrates that the constructed relationship between permeability and porosity in Eq. (6) has certain ability to predict the trend of permeability of the samples from both Longmaxi and Niutitang shale formations. The trends of permeability increase with the increasing porosity have been reflected and the correlation reflects the basic control that grain size exerts on pore size in fine-grained clastic sediments like shale. However, there are still approximately three orders of magnitude difference between the calculated permeability and the measured one (Fig. 10(a)).

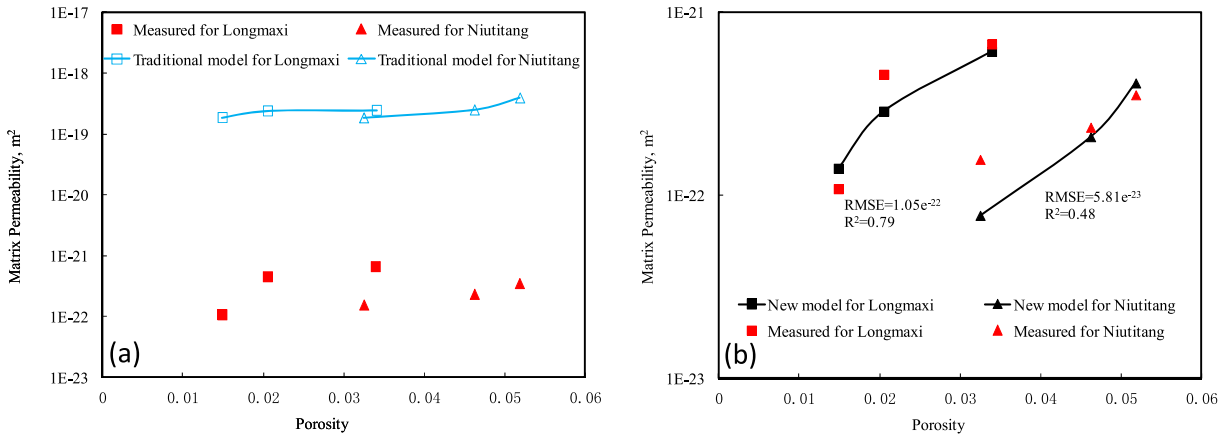

Fig. 10. Comparison of measured, calculated and the fitted permeability of Longmaxi and Niutitang shales (a). Traditional model; (b). New model.

Specifically, the calculated permeability of both Longmaxi and Niutitang shales is higher than the measured one.

The discrepancy between the measured permeability and the calculated value demonstrates that pore spacing may not be the dominant controller of permeability. In addition, the pore spacing cannot be precisely determined due to the constraint of measurement condition and the calculation of permeability through porosity and pore aperture/spacing (Eq. (6)) may not be proper to be applied in rocks other than coal. Since the pore-size distribution has been demonstrated to have significant impacts on porosity and matrix permeability (section 3.1), the relationship between permeability and porosity was modified with consideration of pore-size distribution in the following.

According to Kozeny-Carman equation, permeability has a relationship with porosity and characteristics of pore shape (Revil and Cathles, 1999):

$$k = \frac{\varphi}{2}\left(\frac{V_p}{S}\right)^2 \tag{7}$$

where V_p represents pore volume; and S represents pore surface. For a porous media composed of parallel tubes with equal diameter, the ratio of pore volume to pore surface equals to $R/2$ (R is the average pore radius) and thus permeability is related to the square of the pore radius as follows,

$$k = \frac{\varphi}{2}\left(\frac{R}{2}\right)^2 \tag{8}$$

However, the microscopic pore structure in shale is complicated with dead ends, stagnant regions and isolated pores. Pores may be interconnected through narrow throats which control the transport properties but contribute very little to porosity (Krohn, 1988; Bernabé, 1995). The conventional Kozeny-Carman relationship between permeability and porosity is valid for an ideal situation without consideration of pore geometry, pore connectivity or tortuosity. Therefore, the effective porosity (φ_{eff}) was introduced to reduce the impact of invalid pore space on permeability and to the displace the porosity in Eq. (8) as follows,

$$k = \frac{\varphi_{eff}}{2}\left(\frac{R}{2}\right)^2 \tag{9}$$

Revil and Cathles (1999) pointed out that the effective porosity has a relationship with the electrical formation factor (F):

$$\varphi_{eff} = \frac{1}{F} \tag{10}$$

The electrical potential gradients are concentrated in the throats of the interconnected pore space, which contribute most to the $1/F$. F is related to the porosity and can be expressed by the empirical Archie relationship as follows (Revil and Cathles, 1999; Waxman and Smits, 1968),

$$F = \varphi^{-m} \tag{11}$$

where m is referred to the cementation exponent and varies with pore geometry, ranging from 1 to 4 (Sen et al., 1981). The value of m represents the match of the size of connected pores and throats. Substituting Eqs. (10 and 11) into Eq. (9) obtains the final relationship between permeability and porosity,

$$k = \frac{\varphi^m}{2}\left(\frac{R}{2}\right)^2 = \frac{\varphi^m d^2}{32} \tag{12}$$

where d is the average pore diameter, which can be obtained from the mercury intrusion at laboratory. φ can be obtained from the porosity measurements.

The value of m was investigated in many researches (e.g. Sen et al., 1981; Johnson et al., 1982; Pape et al., 1987; Schwartz et al., 1989). For the material of glass, the value of m would be larger than 2.5 if large pores were connected by narrow throats, while for shales, the value of m depends on the composition of minerals and varies from 2.34 to 4.17 (Revil and Cathles, 1999). In this study, m is 2.45 for Longmaxi samples and 2.95 for Niutitang samples.

It is suggested in some studies that compared with pore aperture/spacing, the pore geometry and pore-size distribution affect permeability more significantly (Chalmers et al., 2012). With the proper selection of m, the permeability calculated through Eq. (12) was applied to match with the measured permeability, as shown in Fig. 10(b). The calculated permeability increases with the increasing porosity for both Longmaxi and Niutitang samples, and the new model can match the experimental data with reasonable accuracy compared with the traditional model. The root-mean-square error (RMSE) was calculated as following,

$$RMSE = \sqrt{\sum_{i=1}^{n}\frac{\left(k^{cal} - k^{\exp}\right)^2}{n}} \tag{13}$$

where k^{cal} represents the calculated permeability from the

proposed model, and k^{exp} represents the measured permeability, n is the number of experimental points. According to Eq. (13), the RMSE is $1.05e^{-22}$ m^2 for the Longmaxi samples and $5.81e^{-23}$ m^2 for the Niutitang samples respectively.

Both the traditional model (as referred to Eq. (6)) and the new model (Eq. (12)) successfully predict the increasing trend of permeability with porosity. However, experimental data are matched better by the new model than by the traditional model probably due to the following two reasons. On the one hand, the new model considers effects of pore-size distribution and pore geometry on the relationship between matrix permeability and porosity through the parameter—*m*. On the other hand, the average pore radius or median pore-throat radius can be relatively precisely measured through mercury intrusion curve while the pore spacing (*a*) used in the traditional model is difficult to measure at laboratory.

The value of *m* represents the effects of pore geometry and pore-size distribution on matrix permeability. *m* is small if the interconnected pore space consists of open cracks while it is large if the size of pores and throats are not matched. In this study, the value of *m* is selected based on the experimental data matching, which is consistent with the above analyses of pore-size distribution and pore structure for the Longmaxi and Niutitang samples. From the analysis in Section 3.1, the difference between the amount of mercury intrusion and extrusion of Niutitang samples is larger than that of the Longmaxi samples, indicating that the pore structures are more complex in the Niutitang shales. The value of *m* for Niutitang samples therefore should be larger.

The control of geological and geochemical characteristics on the shale porosity and permeability is reflected through the control of pore-size distribution and pore geometry. In this study, the effects of pore-size distribution and pore geometry on the relationship between shale matrix permeability and porosity has been taken into account in the new model. However, the simple parameter *m* proposed in this model is not enough to generally represent the impact of all the geological and geochemical factors. The effects of complicated geometry of flow path and each geological and geochemical factor on the relationship of matrix permeability and porosity require more investigation in the future. Meanwhile, the value of *m* needs to be selected according to the rock properties when the model is applied to the non-marine shales since the permeability—porosity relationship established here is mainly based on marine shales.

3.6. Comparison of matrix permeability and plug permeability

The matrix permeability of the Longmaxi shales measured through the Pressure-decay method on crushed samples is compared with the permeability measured through the Pulse-decay method on plug samples, as shown in Fig. 11. The permeability measured with both methods have the same increasing trend of variation with the increasing TOC, whereas the plug permeability is over two orders of magnitude higher than the matrix permeability, which may be caused by several reasons. On the one hand, matrix permeability may be underestimated because the connectivity of the pore network may be damaged in the sample crushing process, resulting in the low matrix permeability. Under this condition, the Pressure-decay method should be modified and proper size should be chosen for the crushed samples. On the other hand, the existence of the natural or man-made fractures with high conductivity may lead to the high permeability of the whole plug since low confining pressure is applied during the plug permeability measurement. Consequently, the Pulse-decay permeability measured on core plugs is not able to represent the matrix permeability and the plug permeability needs to be verified

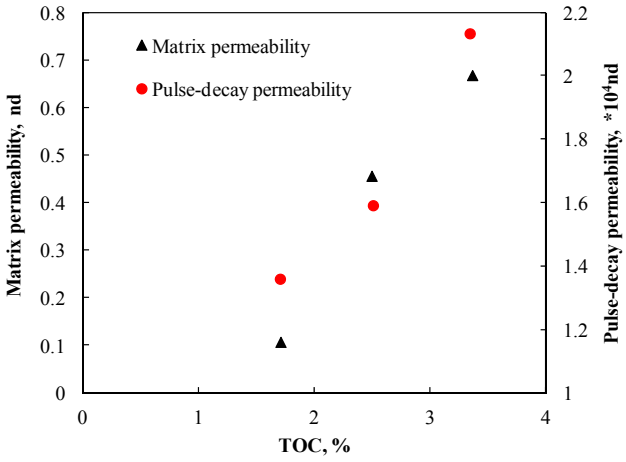

Fig. 11. Comparison of matrix permeability and plug permeability of Longmaxi shale samples.

under the condition of the in-situ stress.

The change of shale permeability with effective stress has significant effect on the long-term gas production. The effect of confining pressure on permeability measured on the plug samples from Niutitang shale is demonstrated in Fig. 12. Four plugs perpendicular to the bedding obtained from outcrop 1 and outcrop 3 (two plugs from each outcrop) were tested to diminish the effect of heterogeneity of the samples in the same direction. It shows similar decreasing trends for the sample $N^{\#}1$ and $N^{\#}1^*$ as well as $N^{\#}3$ and $N^{\#}3^*$, indicating that the heterogeneity perpendicular to the bedding of these samples are not strong, therefore the sample $N^{\#}1^*$ and $N^{\#}3^*$ are primarily analyzed in the following.

Permeability decreases remarkably with the increasing confining pressure for all the four samples. The permeability of sample $N^{\#}3$ and $N^{\#}3^*$ are higher than those of sample $N^{\#}1$ and $N^{\#}1^*$, probably due to the better development of natural or man-made micro fractures or pores in the former samples. Permeability of the sample $N^{\#}3^*$ is 21.54 nD at the confining pressure of 3 MPa, approximately 19 nD higher than that of the sample $N^{\#}1^*$ at the same confining pressure. Permeability decreases sharply to

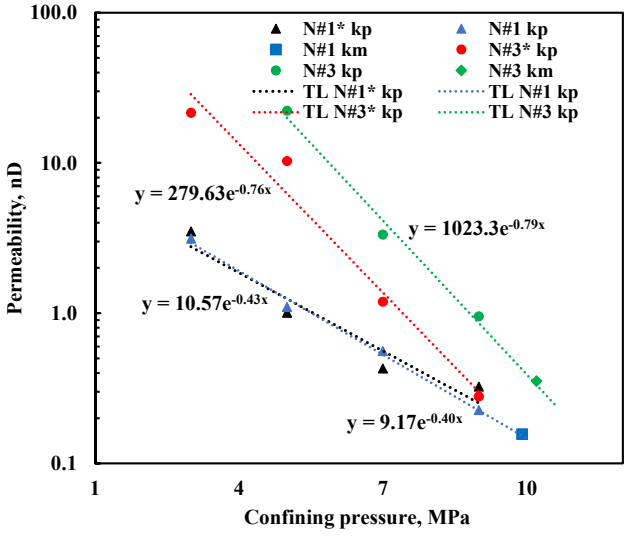

Fig. 12. Comparison of plug permeability at a series of confining pressure and matrix permeability on crushed samples of Niutitang shale (kp represents the plug permeability, km represents the matrix permeability, and TL represents the trend line of experimental plug permeability).

10.26 nD and 1 nD for the sample N#3* and N#1* respectively as the confining pressure increases to 5 MPa, whereas permeability at 9 MPa is not much of difference for these two samples, which stables at 0.27 nD and 0.32 nD respectively.

Permeability decreases by 11.28 nD and 2.50 nD as the confining pressure increases from 3 MPa to 5 MPa, followed by a decrease of 0.91 nD and 0.10 nD from 7 MPa to 9 MPa for the shale sample N#3* and N#1* respectively. Permeability of both samples decreases less in the second increasing interval of confining pressure because the micro fractures and small pores are more difficult to compress compared to the big ones. Moreover, the different decreasing extents of these two samples also indicate that more big pores develop in sample N#3* than in sample N#1* since the permeability decrease in the second confining pressure interval of sample N#1* is much smaller, due to the difficulty of small-pore compression.

Permeability demonstrates an exponential relationship with confining pressure for both Longmaxi and Niutitang shale samples, consistent with the models describing the stress-dependent permeability in coal and other tight formations (Chen et al., 2015; McKee et al., 1988; Palmer and Mansoori, 1996; Shi and Durucan, 2004; Zhang et al., 2008a,b). The exponential coefficients are 0.79, 0.76, 0.43 and 0.40 for the sample N#3, N#3*, N#1* and N#1, respectively, indicating their difference in the porosity sensitivity and pore compressibility. Therefore, permeability of sample N#3* and N#3 are more sensitive to the confining pressure than those of sample N#1* and N#1, implying that the impacts of porosity decrease on permeability of sample N#1* and N#1 are less than those of sample N#3* and N#3. The matrix pores in sample N#1* and N#1 are speculated to contribute more to the permeability compared to the fractures.

The matrix permeability of Niutitang shale samples, which is 0.35 nD and 0.15 nD for sample N#3 and N#1 respectively, was measured under no confining pressure and the value is presented in Fig 12 to compare with the plug permeability. The plug permeability decreases more than one order of magnitude with the increasing confining pressure and the matrix permeability is approximately two orders of magnitude lower than the plug permeability at the confining pressure of 3 MPa.

Since the permeability dependency on the confining pressure is partially caused by the micro fractures compression, the plug permeability has the potential to decrease with further increase of the confining pressure until all the micro fractures are possibly closed. As a consequence, it is speculated that plug permeability is not a representative value of matrix permeability, while permeability at the closing pressure may be proper to be compared with the matrix permeability. According to the trend line of the plug permeability, matrix permeability is approximate to the permeability measured with plug at the confining pressure of 9.90 MPa and 10.20 MPa for the sample N#1 and N#3 respectively, under which condition the connected micro fractures may be partially closed.

Compared to the heterogeneity in the same direction, the effect of anisotropy on permeability should not be neglected. Two plugs were drilled perpendicular and parallel to the beddings respectively from the outcrop #2 of Niutitang shale and permeability in different directions were compared. Shale permeability are direction dependent, with higher values parallel to bedding and lower values perpendicular to the bedding, as shown in Fig. 13, consistent with the observations in other experiments (Mokhtari and Tutuncu, 2015; Pan et al., 2015a,b). Permeability of the sample parallel to the bedding ranges from 4.33 nD to 55.96 nD, which is over one order of magnitude higher than that of the sample perpendicular to the bedding, varying between 0.38 nD and 3.22 nD. This phenomenon reflects factors of material heterogeneity and particle alignment. Material heterogeneity mainly depends on sediment deposition

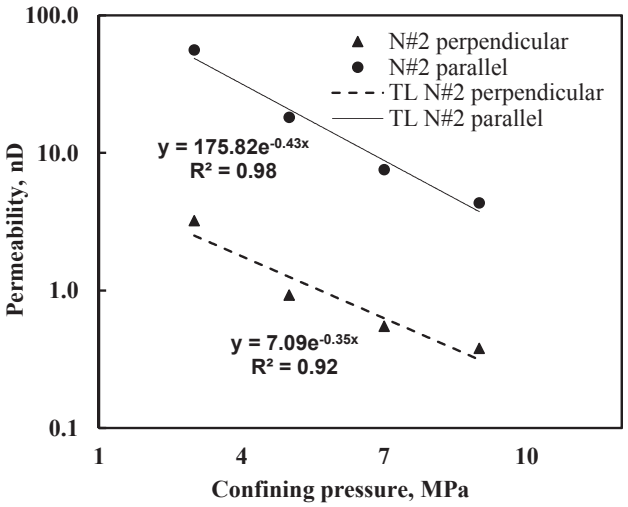

Fig. 13. Comparison of Niutitang shale permeability measured with plug samples perpendicular and parallel to the beddings (TL represents the trend line for experimental data).

(Bennett et al., 1991), while particle alignment results from the subsequent mechanical compaction and clay mineral recrystallization (Aplin et al., 2006; Bolton et al., 2000; Day-Stirrat et al., 2008; Ho et al., 1999).

4. Conclusions

Controls on matrix permeability of the Lower Silurian Longmaxi shale and the Lower Cambrian Niutitang shale were investigated through permeability measurements and a series of geochemical and geological characterization at laboratory. The reasons for the different gas production from these two shale formations were analyzed. Some conclusions are drawn as following:

(1) Matrix permeability and porosity increase with increasing TOC for both the Longmaxi and Niutitang shale.
(2) For the Niutitang shale, matrix permeability is low although porosity is relatively high because matrix permeability is not only determined by porosity but also the pore structure (i.e. pore-size distribution and pore geometry), governed by the geological and geochemical characteristics.
(3) The macropores develop better in the Longmaxi shale while the micropores are more predominant in the Niutitang shale. In addition, the mineral pores develop together with the organic pores which are partially or fully filled by the minerals in the Niutitang shale, resulting in low gas production.
(4) The relationship between permeability and porosity based on the Kozeny-Carman model was modified with the proposal of an indicator *m*, indicating the match of pores and throats, to demonstrate the effects of pore geometry and pore-size distribution on shale permeability. However, the exact estimation of *m* needs to be further studied.
(5) Plug permeability is exponentially proportional to the confining pressure. For Longmaxi and Niutitang shales, matrix permeability measured through Pressure-decay method approaches the plug permeability at the shale closing pressure measured through Pulse-decay method.

Acknowledgements

This work is supported by the Foundation of State Key

Laboratory of Petroleum Resources and Prospecting, China University of Petroleum, Beijing (No. PRP/indep-4-1314); Science Foundation of China University of Petroleum, Beijing (No. 2462014YJRC015); State Key Laboratory of Geomechanics and Geotechnical Engineering, Institute of Rock and Soil Mechanics, Chinese Academy of Sciences (No. Z014006); and State Key Laboratory of Coal Resources and Safe Mining (China University of Mining and Technology) (No. SKLCRSM14KFB09).

References

Aplin, A.C., Yang, Y., Hansen, S., 1995. Assessment of β, the compression coefficient of mudstones and its relationship with detailed lithology. Mar. Pet. Geol. 12, 955–963.
Aplin, A.C., Matenaar, I.F., McCarty, D., van der Pluijm, B.A., 2006. Influence of mechanical compaction and clay mineral diagenesis on the MICROFABRIC and pore-scale properties of Deep water Gulf of Mexico mudstones. Clays Clay Miner. 54, 501–515.
Bennett, R.H., O'Brien, N.R., Hulbert, M.H., 1991. Determinants of Clay and Shale Microfabric Signatures: Processes and Mechanisms. Springer, New York, pp. 5–32.
Bernabé, Y., 1995. The transport properties of networks of cracks and pores. J. Geophys. Res. 100, 4231–4241.
Berryman, J.G., 1992. Effective stress for transport properties in inhomogeneous porous rock. J. Geophys. Res. 97, 17,409–17,424.
Bethke, C.M., 1989. Modeling subsurface flow in sedimentary basins. Geol. Rundsch. 78, 129–154.
Bolton, A.J., Maltman, A.J., Fisher, Q., 2000. Anisotropic permeability and bimodal pore-size distributions of fine-grained marine sediments. Mar. Pet. Geol. 17 (6), 657–672.
Borst, R.L., 1982. Some effects of compaction and geological time on the pore parameters of argillaceous rocks. Sedimentology 29, 291–298.
Brace, W., Walsh, J.B., Frangos, W.T., 1968. Permeability of granite under high pressure. J. Geophys. Res. 73 (6), 2225–2236.
Carles, P., Egermann, P., Lenormand, P., Lombard, J.M., 2007. Low permeability measurements using steady-state and transient methods. In: SCA Paper 2007–07 Presented at International Symposium of the Society of Core Analysis, Calgary; 10–14 September.
Chalmers, G.R., Ross, D.J., Bustin, R.M., 2012. Geological controls on matrix permeability of Devonian Gas Shales in the Horn River and Liard basins, northeastern British Columbia, Canada. Int. J. Coal Geol. 103, 120–131.
Chen, S., Zhu, Y., Qin, Y., Wang, H., Liu, H., Fang, J., 2014. Reservoir evaluation of the Lower Silurian Longmaxi Formation shale gas in the southern Sichuan Basin of China. Mar. Pet. Geol. 57, 619–630.
Chen, D., Pan, Z., Ye, Z., 2015. Dependence of gas shale fracture permeability on effective stress and reservoir pressure: model match and insights. Fuel 139, 383–392.
Cui, A., Brezovski, R., 2013. Laboratory permeability measurements of unconventional reservoirs: useless or full of information? A Montney example from the Western Canadian Sedimentary Basin. In: SPE Paper 167047. SPE Unconventional Resources Conference and Exhibition-asia Pacific, 11–13 November, Brisbane, Australia.
Cui, X., Bustin, A.M.M., Bustin, R.M., 2009. Measurements of gas permeability and diffusivity of tight reservoir rocks: different approaches and their applications. Geofluids 9, 208–223.
Cui, A., Wust, R., Nassichuk, B., Glover, K., Brezovski, R., Twemlow, C., 2013. A nearly complete characterization of permeability to hydrocarbon gas and liquid for unconventional reservoirs: a challenge to conventional thinking. In: SPE Paper 168730 Presented at the SPE Unconventional Resources Technology Conference, Denver; 12–14 August.
Dai, J., Zou, C., Liao, S., Dong, D., Ni, Y., Huang, J., Wu, W., Gong, D., Huang, S., Hu, G., 2014. Geochemistry of the extremely high thermal maturity Longmaxi shale gas, southern Sichuan Basin. Org. Geochem. 74, 3–12.
Day-Stirrat, R.J., Aplin, A.C., Srodon, J., van der Pluijm, B.A., 2008. Diagenetic reorientation of phyllosilicate minerals in Paleogene mudstones of the Podhale Basin, southern Poland. Clays Clay Miner. 56, 98–109.
Dewhurst, D.N., Aplin, A.C., Sarda, J.P., Yang, Y.L., 1998. Compaction-driven evolution of poroperm in natural mudstones: an experimental study. J. Geophys. Res. 103, 651–661.
Dewhurst, D.N., Yang, Y., Aplin, A.C., 1999a. Permeability and fluid flow in natural mudstones. Geol. Soc. Lond. Spec. Publ. 158 (1), 23–43.
Dewhurst, D.N., Yang, Y., Aplin, A.C., 1999b. Permeability and fluid flow in natural mudstones. In: Aplin, A.C., Fleet, A.J., Macquaker, J.H.S. (Eds.), Muds and Mudstones: Physical and Fluid Flow Properties, Geological Society of London Special Publication, 158, pp. 23–43.
Feng, Y., Zhengfu, N., Qing, W., Huiqing, L., Shidong, Z., Hongmei, L., 2013. Integrated Study of Reservoir Characteristics of a Shale Gas Reservoir: a Case Study from Sichuan Basin of China. SPE Paper 165870.
Ghanizadeh, A., Gasparik, M., Amann-Hildenbrand, A., Gensterblum, Y., Krooss, B., 2013. Lithological controls on matrix permeability of organic-rich shales: an experimental study. Energy Procedia 40, 127–136.
Ghanizadeh, A., Gasparik, M., Amann-Hildenbrand, A., Gensterblum, Y., Krooss, B.M., 2014a. Experimental study of fluid transport processes in the matrix system of European organic-rich shales: I. Scandinavian Alum Shale. Mar. Pet. Geol. 51, 79–99.
Ghanizadeh, A., Gasparik, M., Amann-Hildenbrand, A., Gensterblum, Y., Krooss, B.M., Littke, R., 2014b. Experimental study of fluid transport processes in the matrix system of the European organic-rich shales: II. Posidonia Shale (Lower Toarcian, northern Germany). Int. J. Coal Geol. 123, 20–33.
Ghanizadeh, A., Aquino, S., Haeri-Ardakani, O., Sanei, H., Clarkson, C.R., 2015. A comparison of shale permeability coefficients derived using multiple non-steady-state measurement techniques: examples from the Duvernay Formation, Alberta (Canada). Fuel 140 (15), 371–387.
Ho, N.C., Peacor, D.R., van der Pluijm, B.A., 1999. Preferred orientation of phyllosilicates in Gulf Coast mudstones and relation to the smectite-to-illite transition. Clays Clay Miner. 47, 495–504.
Johnson, D.L., Plona, T., Scala, C., Pasierb, F., Kojima, H., 1982. Tortuosity and acoustic slow waves. Phys. Rev. Lett. 49 (25), 1840.
Jones, S.C., 1994. A new, fast, accurate pressure-decay probe permeameter. SPE Form. Eval. 9, 193–199.
Jones, S.C., 1997. A technique for faster pulse-decay permeability measurements in tight rocks. SPE Form. Eval. 12, 19–26.
Krohn, C.E., 1988. Fractal measurements of sandstones, shales, and carbonates. J. Geophys. Res. 93, 3297–3305.
Kwon, O., Kronenberg, A.K., Gangi, A.F., Johnson, B., Herbert, B.E., 2004. Permeability of illite-bearing shale: 1. Anisotropy and effects of clay content and loading. J. Geophys. Res. 109 (B10205), 1–19.
Lapierre, C., Leroueil, S., Locat, J., 1990. Mercury intrusion and permeability of Louiseville clay. Can. Geotech. J. 27 (6), 761–773.
Lash, G.G., Engelder, T., 2005. An analysis of horizontal microcracking during catagenesis: example from the Catskill delta complex. Am. Assoc. Pet. Geol. Bull. 89, 1433–1449.
Liang, D.G., Guo, T.L., Chen, J.P., Zeng, B.L., Zhao, Z., 2008. Some progresses on studies of hydrocarbon generation and accumulation in marine sedimentary regions, Southern China (Part 1): distribution of four suits of regional marine source rocks. Mar. Orig. Pet. Geol. 13 (2), 1–16 (in Chinese with English abstract).
Loucks, R.G., Reed, R.M., Ruppel, S.C., Jarvie, D.M., 2009. Morphology, genesis, and distribution of nanometer-scale pores in siliceous mudstones of the Mississippian Barnett Shale. J. Sediment. Res. 79 (12), 848–861.
Luffel, D.L., Hopkins, C.W., Holditch, S.A., Schettler, P.D., 1993. Matrix permeability measurement of gas productive shales. In: SPE Paper 26633 Presented at the Society of Petroleum Engineers Annual Technical Conference and Exhibition, Houston, Texas; 3–6 October.
Ma, Y., Zhong, N., Li, D., Pan, Z., Cheng, L., Liu, K., 2015. Organic matter/clay mineral intergranular pores in the Lower Cambrian Lujiaping Shale in the north-eastern part of the upper Yangtze area, China: a possible microscopic mechanism for gas preservation. Int. J. Coal Geol. 137, 38–54.
McKee, C.R., Bumb, A.C., Koenig, R.A., 1988. Stress-dependent permeability and porosity of coal and other geologic formations. SPE Form. Eval. 81–91.
Mesri, G., Olson, R.E., 1971. Mechanisms controlling the permeability of clays. Clays Clay Miner. 19, 151–158.
Metwally, Y.M., Sondergeld, C., 2011. Measuring low permeabilities of gas-sands and shales using a pressure transmission technique. Int. J. Rock Mech. Min. Sci. 48 (7), 1135–1144.
Mokhtari, M., Tutuncu, A.N., 2015. Characterization of anisotropy in the permeability of organic-rich shales. J. Pet. Sci. Eng. 133, 496–506.
Nagaraj, T.S., Pandian, N.S., Narasimha Raju, P.S.R., 1994. Stress-state-permeability relations for overconsolidated clays. Geotechnique 44, 349–352.
Nelson, P.H., 1994. Permeability-porosity relationships in sedimentary rocks. Log Anal. 35 (03).
Palmer, I., Mansoori, J., 1996. How permeability depends on stress and pore pressure in coalbeds: a new model. In: SPE Annual Technical Conference and Exhibition. Society of Petroleum Engineers.
Pan, Z., Connell, L.D., 2012. Modelling permeability for coal reservoirs: a review of analytical models and testing data. Int. J. Coal Geol. 92, 1–44.
Pan, Z., Connell, L.D., 2015. Reservoir simulation of free and adsorbed gas production from shale. J. Nat. Gas Sci. Eng. 22, 359–370.
Pan, Z., Connell, L.D., Camilleri, M., 2010. Laboratory characterisation of coal reservoir permeability for primary and enhanced coalbed methane recovery. Int. J. Coal Geol. 82, 252–261.
Pan, S., Zou, C., Yang, Z., Dong, D., Wang, Y., Wang, S., Wu, S., Huang, J., Liu, Q., Wang, D., 2015a. Methods for shale gas play assessment: a comparison between Silurian Longmaxi shale and Mississippian Barnett shale. J. Earth Sci. 26 (2), 285–294.
Pan, Z., Ma, Y., Connell, L.D., Down, D.I., Camilleri, M., 2015b. Measuring anisotropic permeability using a cubic shale sample in a triaxial cell. J. Nat. Gas Sci. Eng. 26, 336–344.
Pape, H., Riepe, L., Schopper, J.R., 1987. Interlayer conductivity of rocks—a fractal model of interface irregularities for calculating interlayer conductivity of natural porous mineral systems. Colloids Surfaces 27 (4), 97–122.
Pu, B., Dong, D., Zhao, J., Er, C., Huang, J., 2015. Differences between marine and terrestrial shale gas accumulation: taking longmaxi shale Sichuan Basin and Yanchang Shale Ordos Basin as examples. Acta Geol. Sin. 89, 200–206 (English Edition).
Revil, A., Cathles, L., 1999. Permeability of shaly sands. Water Resour. Res. 35 (3), 651–662.

Schlomer, S., Krooss, B.M., 1997. Experimental characterisation of the hydrocarbon sealing efficiency of cap rocks. Mar. Pet. Geol. 14, 565–580.
Schwartz, L.M., Sen, P.N., Johnson, D.L., 1989. Influence of rough surfaces on electrolytic conduction in porous media. Phys. Rev. B 40 (4), 2450.
Sen, P., Scala, C., Cohen, M., 1981. A self-similar model for sedimentary rocks with application to the dielectric constant of fused glass beads. Geophysics 46 (5), 781–795.
Shi, J., Durucan, S., 2004. Drawdown induced changes in permeability of coalbeds: a new interpretation of the reservoir response to primary recovery. Transp. porous media 56, 1–16.
Soeder, D.J., 1988. Porosity and permeability of Eastern Devonian gas shale. SPE Form. Eval. 3 (1), 116–124.
Suarez-Rivera, R., Chertov, M., Willberg, D.M., Green, S.J., Keller, J., 2012. Understanding permeability measurements in tight shales promotes enhanced determination of reservoir quality. In: SPE Paper 162816 Presented at the SPE Canadian Unconventional Resources Conference, Calgary; 30 October–1 November, 2012.
Tian, H., Pan, L., Zhang, T., Xiao, X., Meng, Z., Huang, B., 2015. Pore characterization of organic-rich Lower Cambrian shales in Qiannan depression of Guizhou Province, Southwestern China. Mar. Pet. Geol. 62, 28–43.
Tinni, A., Fathi, E., Agarwal, R., Sondergeld, C., Akkutlu, Y., Rai, C., 2012. Shale permeability measurements on plugs and crushed samples. In: SPE Paper 162235 Presented at the Society of Petroleum Engineers Canadian Unconventional Resources Conference, Calgary; 30 October–1 November, 2012.
U.S. Energy Information Administration, 2013. Technically Recoverable Shale Oil and Shale Gas Resources: an Assessment of 137 Shale Formations in 41 Countries outside the United States. June, 2013.
Walsh, J.B., Brace, W.F., 1984. The effect of pressure on porosity and the transport properties of rock. J. Geophys. Res. 89, 9425–9431.
Wang, F.Y., Guan, J., Feng, W.P., Bao, L.Y., 2013a. Evolution of overmature marine shale porosity and implication to the free gas volume. Pet. Explor. Dev. 40 (6), 819–824.
Wang, L., Dumesnil, J., Deng, S., Chong, K.K., Lv, Z., Wang, Q., 2013b. Sichuan Basin Longmaxi Shale Gas Stimulation and Completion Case Study. SPE paper 167006.
Wang, Q., Lv, Z., Chong, K.K., Dumesnil, J.P., Deng, S., Wang, L., 2013c. China Shale Gas Exploration: Early Sichuan Basin Longmaxi Shale Gas Stimulation and Completion Case Study. SPE paper 166746.
Wang, Y., Zhai, G., Bao, S., Ren, S., Ge, M., Zhou, Z., 2015. Latest progress and trend forecast of China's Shale gas exploration and development. Acta Geol. Sin. 89, 211–213 (English Edition).
Wang, H.T., 2014. Performance of multiple fractured horizontal wells in shale gas reservoirs with consideration of multiple mechanisms. J. Hydrol. 510, 299–312.
Waxman, M., Smits, L., 1968. Electrical conductivities in oil-bearing shaly sands. Soc. Pet. Eng. J. 8 (2), 107–122.
Wei, C., Wang, H., Sun, S., Xiao, Y., Zhu, Y., Qin, G., 2012. Potential Investigation of Shale Gas Reservoirs, Southern China. SPE Paper 162828.
Wu, Y., Fan, T., Zhang, J., Jiang, S., Li, Y., Zhang, J., Xie, C., 2014. Characterization of the Upper Ordovician and Lower Silurian Marine Shale in Northwestern Guizhou Province of the Upper Yangtze Block, South China. Implic. Shale Gas Potential Energy & Fuels 28 (6), 3679–3687.
Yang, Y., Aplin, A.C., 1998. Influence of lithology and compaction on the pore size distribution and modelled permeability of some mudstones from the Norwegian margin. Mar. Pet. Geol. 15 (2), 163–175.
Yang, Y., Aplin, A.C., 2007. Permeability and petrophysical properties of 30 natural mudstones. J. Geophys. Res. 112, 1–14.
Yang, C., Xu, H., 2015. Accumulation conditions of Shale Gas from the Lower Cambrian Niutitang formation in Central Guizhou Uplift and its periphery. Acta Geol. Sin. 89, 290–292 (English Edition).
Yang, F., Ning, Z., Liu, H., 2014. Fractal characteristics of shales from a shale gas reservoir in the Sichuan Basin, China. Fuel 115, 378–384.
Yang, F., Ning, Z., Wang, Q., Liu, H., 2015a. Pore structure of Cambrian shales from the Sichuan Basin in China and implications to gas storage. Mar. Pet. Geol. 70, 14–26.
Yang, X., Fan, T., Wu, Y., 2015b. Lithofacies and Cyclicity of the Lower Cambrian Niutitang Shale in the Mayang Basin of Western Hunan, South China. J. Nat. Gas Sci. Eng. 28, 74–86.
Zhang, H., Liu, J., Elsworth, D., 2008a. How sorption-induced matrix deformation affects gas flow in coal seams: a new FE model. Int. J. Rock Mech. Min. Sci. 45, 1226–1236.
Zhang, J.C., Nie, H.K., Xu, B., Jiang, S.L., Zhang, P.X., 2008b. Geological condition of shale gas accumulation in Sichuan Basin. Nat. Gas Ind. 28 (2), 157–159.
Zhang, J.C., Li, Y.X., Nie, H.K., Long, P.Y., Tang, Y., Tang, X., Jiang, W.L., 2010. Geologic setting and drilling effect of the shale cored well Yuye-1, Pengshui County of Chongqing. Nat. Gas Ind. 30 (12), 114–118.
Zou, C.N., Zhu, R.K., Bai, B., Zhi, Y., Songtao, W.U., Ling, S.U., 2011. First discovery of nano-pore throat in oil and gas reservoir in china and its scientific value. Acta Petrol. Sin. 27 (6), 1857–1864.